Materials Science in Semiconductor Processing 170 (2024) 107981

Contents lists available at ScienceDirect

Materials Science in Semiconductor Processing

journal homepage: www.elsevier.com/locate/mssp

Effect of aluminum content on plasma resistance and contamination particle generation in yttrium aluminum oxide coatings

Jongho So [a,b,1], Eunmi Choi [c,1], Minjoong Kim [b], Dongjin Lee [c], Jungpil Seo [c], Seonjeong Maeng [b], Chin-Wook Chung [a], Ju-Young Yun [b,d,*], Song-Moon Suh [c,**]

[a] Department of Electrical Engineering, Hanyang University, Seoul, 04763, Republic of Korea
[b] Vacuum Materials Measurement Team, Korea Research Institute of Standards and Science, Daejeon, 34113, Republic of Korea
[c] Defect Engineering Group, SK hynix Inc., Icheon, 17336, Republic of Korea
[d] Nanoscience and Technology, University of Science and Technology, Daejeon, 34113, Republic of Korea

ARTICLE INFO

Keywords:
Contamination particle
Yttrium aluminum oxide
Yttrium aluminum garnet
Atmospheric plasma spray

ABSTRACT

Yttrium aluminum oxide (YAO) has garnered interest due to its ability to protect the interior parts of process chambers from the corrosive effects of fluorine-based plasma. This ability is attributed to its low melting point, which enhances the internal bonding capabilities of the atmospheric plasma spray (APS) method. We explored the resistance of YAO coatings, with varying yttrium-to-aluminum content ratios, to fluorine-based plasma. These coatings were applied using the APS method and subsequently subjected to NF_3/O_2 gas. Our results revealed that a higher Al content ratio resulted in a decreased number of defects within the coating, which also led to selective etching at the initial Al_2O_3-rich sites, primarily creating relatively weak Al-F bonds and smaller particles. In particular, selecting an appropriate yttrium-to-aluminum content ratio significantly reduced the coating defects and enhanced the etch rate compared to coatings with a higher yttrium content ratio. This improvement was attributed to the balanced presence of Al-F and Y-F bonds. Furthermore, for coatings rich with the yttrium aluminum garnet (YAG) phase, the resistance to fluorine-based plasma was primarily influenced by the thickness of the APS-Y_2O_3 layer. This layer, used to augment adhesion to parts, relies on the low-temperature crystallization features of YAG. The findings of this study offer valuable insights for optimizing YAG coating in dry-etching processes requiring high-density APS coatings.

1. Introduction

Fluorine-based gas plasma is widely utilized for isotropic etching via substrate bombardment with fluorine atoms, including radicals, ions, and ultraviolet photons [1,2]. However, the highly reactive generated fluorine atoms corrode the internal chamber parts, a concern particularly relevant to semiconductor manufacturing processes [3,4]. As the size of the semiconductor equipment chamber expands with the Si wafer, particle generation due to corrosion becomes a major issue [5]. Ceramic coatings are often employed to safeguard the internal chamber parts from fluorine-based plasma corrosion owing to their high chemical stability, hardness, dielectric strength, and resistance [6,7]. However, developing successful ceramic coatings typically requires high-temperature environments owing to the high melting points of ceramics. The atmospheric plasma spray (APS) method is widely preferred for coating internal chamber parts, owing to its ability to easily regulate the coating thickness and high ceramic coating speed [8]. However, APS coatings are prone to defects, such as pores and cracks of various sizes. These defects originate from partially unmelted raw powder particles nestled between contiguous splats [9], directly contributing to plasma resistance degradation [10].

Various materials have been used in ceramic coatings, including Y_2O_3 [11], YOF [12], and yttrium aluminum garnet (YAG) [13,14]. Since its introduction by Fujita et al., in 2005 [15], YAG has become a favored coating for internal chamber parts. This preference stems from its ability to enhance plasma resistance properties by reducing the melting point of raw powder particles without compromising the high plasma resistance of Y_2O_3 and decreasing defect generation, a common

* Corresponding author. Vacuum Materials Measurement Team, Korea Research Institute of Standards and Science (KRISS), Daejeon, 34113, Republic of Korea.
** Corresponding author. Defect Engineering Group, SK hynix Inc., Icheon, 17336, Republic of Korea.
E-mail addresses: jyun@kriss.re.kr (J.-Y. Yun), songmoon.suh@sk.com (S.-M. Suh).
[1] These authors contributed equally to this work.

https://doi.org/10.1016/j.mssp.2023.107981
Received 14 August 2023; Received in revised form 27 October 2023; Accepted 10 November 2023
Available online 19 November 2023

issue with APS coatings. However, certain challenges, particularly issues related to the selective etching of Al_2O_3-rich sites and adhesion to parts, remain in applying YAG as a coating for internal chamber parts. Numerous studies have been conducted on the selective etching of Al_2O_3-rich sites. Park et al. exposed APS-coated Al_2O_3, Y_2O_3, YOF, and YAG films to CF_4/O_2 plasma, observing changes in the ceramic coating. Their study confirmed that YAG undergoes minimal chemical change by fluorine-based plasma, with etching occurring along grain boundaries and most erosion occurring at Al_2O_3-rich sites [16]. Huang et al. exposed an APS-YAG coating to an $Ar/CF_4/O_2$ mixed gas plasma generated by capacitively coupled plasma (CCP). They demonstrated that etching products were preferentially formed on semi-molten particle surfaces, within pores, and at the full melting zone edge. These etching traces were subsequently removed by ion bombardment. They also demonstrated that only AlF_3 was present on the YAG coating surface at the onset of etching, with ion bombardment removing some AlF_3 and the remaining AlF_3 being covered by YO_xF_y, preventing further AlF_3 formation [17]. Tan et al. demonstrated that increasing the aluminum content in a YAG coating improved its mechanical properties and confirmed the Al_2O_3-rich site-selective reaction in a plasma environment, consistent with the findings of Park et al. However, the weight loss rate of percolation theory YAG did not proportionally correspond to the aluminum content [18].

Interface adhesion challenges between YAG coatings and internal chamber parts can cause major process accidents owing to the coating peeling off of the parts. Therefore, the adhesion between parts and the coating interface is a crucial factor affecting the reliability of the coating. However, to the best of our knowledge, no previous studies have investigated this aspect. Strategies for mitigating adhesion issues between YAG coatings and the part interface include using Y_2O_3 as a bonding layer or employing coatings dominated by the yttrium aluminum monoclinic (YAM) phase, a phase richer in yttrium compared to YAG.

We investigated the properties of plasma resistance and defect occurrence in APS-YAG and APS-YAM coatings within NF_3-based plasma environments to determine their correlation with selective etching at Al_2O_3-rich sites. Moreover, we developed a YAG coating optimized for internal chamber parts by comparing the variations in plasma resistance characteristics and defect formation levels relative to the YAG-bonded layer.

2. Materials and methods

We applied three types of coatings with varying yttrium and aluminum content ratios to an aluminum 6061 alloy substrate with a thickness of 150 μm using the APS method. X-ray photoelectron spectroscopy was utilized to analyze the yttrium content ratio of each coating, resulting in ratios of 43 %, 69 %, and 85 %. These coatings are henceforth referred to as 0.43 YAO, 0.69 YAO, and 0.85 YAO, respectively (Table 1). The 0.69 YAO and 0.85 YAO coatings with the highest yttrium content ratio do not employ a separate bonding layer. Conversely, the 0.43 YAO coating with the lowest yttrium content ratio incorporates an 80 μm APS-Y_2O_3 layer to enhance adhesion to the substrate.

To assess the plasma resistance of the coating, we utilized a custom-built CCP-type etching device capable of measuring contamination particles generated by plasma exposure in real time (Fig. 1). The specifics of the contamination particles evaluation apparatus used in this study have been detailed in previous experiments [19,20]. The plasma process conditions involved a 10:1 ratio of NF_3/O_2 mixed gas, with 250 W of RF power applied for 1 h, followed by cooling for 0.5 h (plasma off). This sequence was repeated thrice. Each coating was evaluated using X-ray diffraction (XRD, SmartLab, RIGAKU), field-emission scanning electron microscopy (FE-SEM), and energy dispersive spectrometry (EDS, BRUKER, FlatQUAD) before and after the plasma resistance assessment. In addition, the ImageJ program (ver.1.53e, 64-bit) was used to analyze the porosity of the YAO films cross-sectional morphologies.

Furthermore, a pull test was conducted to analyze the effect of the bonding layer thickness on the adhesion between the YAG coating and the substrate. The total coating thickness, including the bonding layer, was 150 μm. We prepared coatings with bonding layer to YAG coating ratios of 1:14, 1:6.5, 1:4, 1:2.75, and 1:2. The coatings demonstrating the best properties were selected and exposed for 1 h to the previously used NF_3/O_2 mixed gas plasma environment. Subsequently, a cleaning process was performed using an acid-based mixed cleaning solution to remove process byproducts on the surface. This plasma exposure and cleaning sequence was repeated twice to evaluate the plasma resistance.

Table 1
Details of the yttrium aluminum oxide (YAO) coating.

	0.43 YAO	0.69 YAO	0.85 YAO
Y atomic% rate	0.43	0.69	0.85
Al atomic% rate	0.57	0.31	0.15
Thickness	140.1 μm ± 4.2 μm	143.2 μm ± 2.1 μm	141.8 μm ± 7.2 μm
Adhesion layer	70.2 μm ± 6.8 μm	-	-

3. Results and discussion

3.1. Coating characterization

Fig. 2 displays the normalized XRD patterns of the three different coatings, each with varying yttrium and aluminum contents. The 0.69 YAO and 0.85 YAO coatings, with relatively high yttrium content ratios, exhibited very similar XRD patterns, with YAM being the dominant phase. Moreover, there was an yttrium aluminum perovskite (YAP)

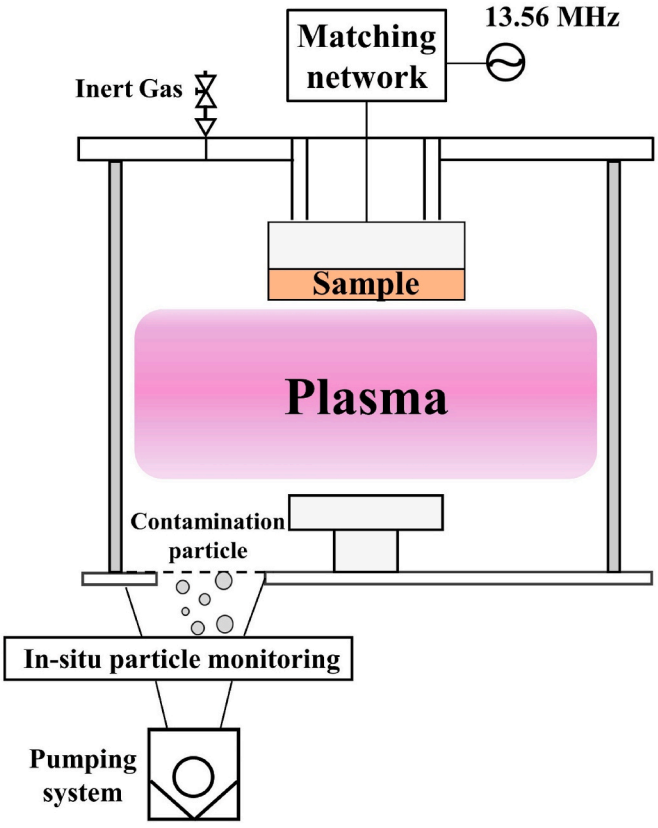

Fig. 1. Schematic of the in-situ particle monitoring system.

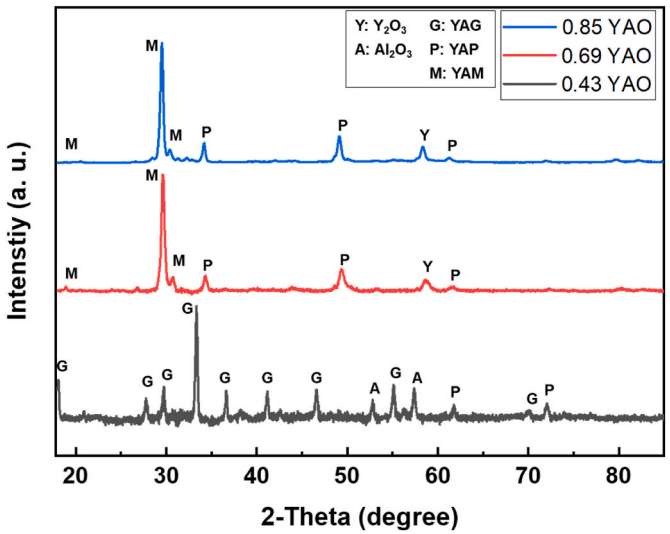

Fig. 2. XRD patterns of YAO coatings.

phase present with an yttrium content ratio lower than that of YAM and higher than that of YAG. Conversely, 0.43 YAO, with a high aluminum content ratio, was relatively less crystalline than 0.69 and 0.85 YAO, and a pattern related to Al_2O_3 and YAG was observed. According to the research by Lang Li et al., the APS process, with its high cooling rate, inhibits the nucleation of YAG droplets during solidification, promoting the formation of an amorphous phase in the coating. However, since the coating surface is continuously exposed to the plasma plume, the temperature of sample steadily increases, leading to a reduction in the degree of undercooling in the droplets as they approach the surface [21]. In the case of 0.43 YAO, it is coated on top of the bonding layer, resulting in a thinner coating layer compared to the other two YAO types. Consequently, the exposure time to the plasma plume is shorter, leading to a faster cooling rate in the droplets, which appears to contribute to its lower crystallinity compared to the other two YAO types.

The yttrium-to-aluminum ratio alters the phase and affects the surface and cross-sectional morphology of the coating. Al_2O_3 has a melting point of 2072 °C and Y_2O_3 has a melting point of 2410 °C. YAG has a lower melting point than Y_2O_3 because of its lower yttrium content, leading to a more efficient melting [17,22]. The surface of 0.43 YAO, which has the highest aluminum content ratio, exhibits more efficient raw powder melting than 0.69 and 0.85 YAO (Fig. 3). Moreover, the cross-sectional morphology reveals different defect characteristics of porosity, cracks, and unmelted powder within the coating (Fig. 4). Despite having a higher aluminum content ratio than 0.69 YAO and 0.85 YAO, the 0.43 YAO did not exhibit the expected enhanced cross-sectional morphology. It displayed larger porosity and crack than 0.69 YAO. The porosities of 0.43 YAO, 0.69 YAO, and 0.83 YAO, as measured using the ImageJ, an image analysis program, were 3.3 %, 1.3 %, 2.2 %, respectively. This discrepancy is likely due to the presence of the APS-Y_2O_3 layer used as the bonding layer. Therefore, for a high-quality YAG coating, it is crucial to eliminate the bonding layer or minimize its influence. This is discussed later in this study. The 0.69 YAO presents the optimal cross-sectional morphology. However, microcracks and the partial presence of Al_2O_3 or YAP, with a lower yttrium content ratio than YAM, resulted in significant inhomogeneity in the coating composition distribution. The 0.85 YAO visibly displayed the presence of unmelted raw powder and, compared to the other two

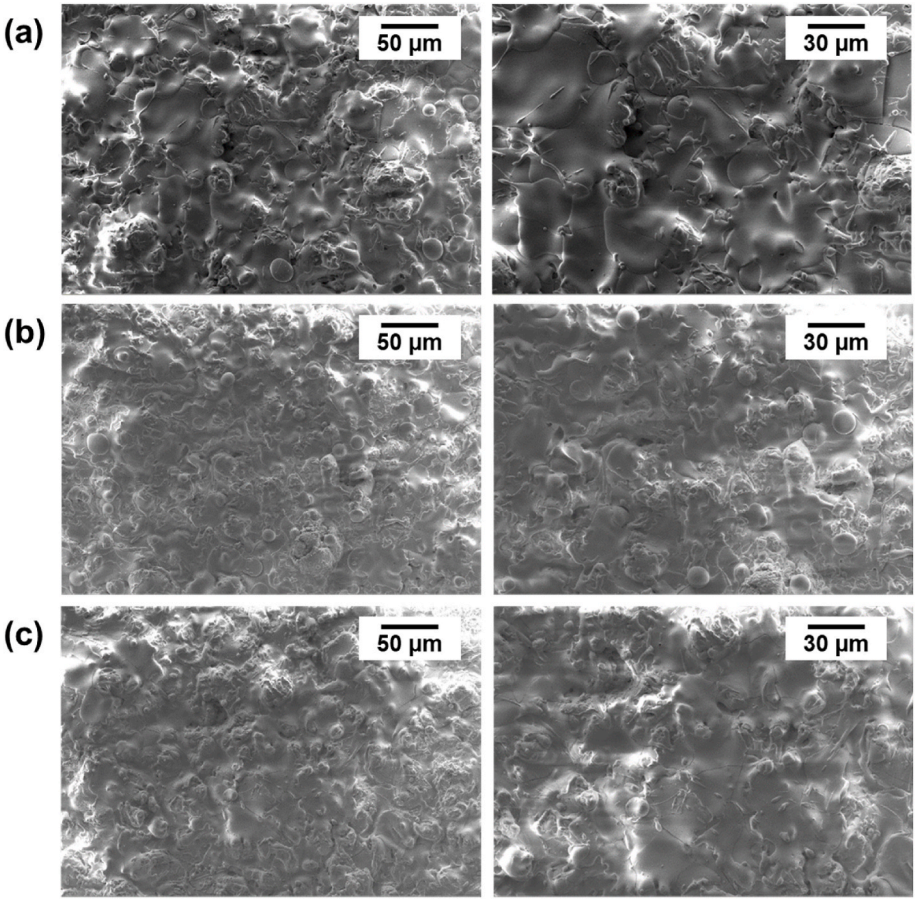

Fig. 3. FE-SEM images of the surface of YAO coatings: (a) 0.43 YAO, (b) 0.69 YAO, and (c) 0.85 YAO.

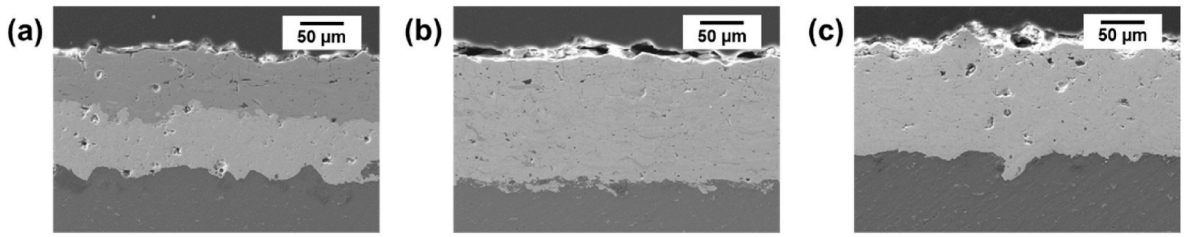

Fig. 4. FE-SEM images of the cross-sectional morphology of YAO coatings: (a) 0.43 YAO, (b) 0.69 YAO, and (c) 0.85 YAO.

YAO types, exhibited large porosity. Furthermore, although less distinct than 0.69 YAO, a compositional inhomogeneity was observed. The uneven composition distribution of YAO coatings is thought to stem from the differing melting points of Al_2O_3 and Y_2O_3 during the APS process.

3.2. Investigation of plasma-resistance characteristics in 0.43, 0.69, and 0.85 YAO

The most significant property impacted by the yttrium and aluminum content ratio in YAG used as a coating for internal chamber parts is the plasma resistance to fluorine-based plasma. The color change in the coating before and after 3 h of exposure to the NF_3/O_2 gas plasma environment indicated that a lower yttrium content ratio resulted in a more pronounced yellowish hue (Fig. 5). This color shift is caused by an increase in oxygen defect concentration resulting from the reaction with -F and the light scattering effect caused by etching [23]. Therefore, we anticipate that lower yttrium content ratios are associated with greater changes elicited by the NF_3/O_2 gas plasma exposure.

Fig. 6 shows the contamination particle count, measured using particles monitoring sensor when the YAO coating was exposed to NF_3/O_2 gas plasma for 3 h, split into three cycles of 1 h each. Fig. 7 illustrates the thickness of the YAO coating before and after the NF_3/O_2 gas plasma exposure. After a cumulative 3-h NF_3/O_2 gas plasma exposure, 0.43 YAO, 0.69 YAO, and 0.85 YAG generated 1597, 1587, and 513 particles, respectively, and their thickness decreased by 14.7 μm, 7.5 μm, and 8.3 μm, respectively. Evaluating particle generation behavior throughout the NF_3/O_2 gas plasma exposure cycles, the total number of particles generated over the three cycles, and the etching thickness, it is possible to predict the distinct behavior of each coating depending on the yttrium content ratio.

The 0.43 YAO generated the highest number of particles compared to the other two YAO types. Additionally, it demonstrated the greatest change in particle generation relative to the thickness change and each cycle. This is attributed to the initial reaction between fluorine plasma and YAG coating, where a rapid reaction between AlO_x sites and -F occurs, followed by the removal of AlF_x via ion bombardment, as indicated in the work of Huang et al. [17]. The highest number of particles was observed during the initial plasma etching cycle. The second plasma etching cycle displayed lower particle generation than the first, indicating more stable plasma resistance characteristics. This was likely because of the coating surface being shielded by YO_xF_y, a mechanism that suppresses subsequent AlF_3 formation [17], and the swift removal of the incomplete surface coating formed due to the absence of a hammering effect in the first plasma etching cycle [24]. Selective AlF_x removal was observed in the EDS image post exposure to the NF_3/O_2 gas plasma (Fig. 8a). In the third cycle, the plasma resistance characteristics remained stable for approximately 20 min, followed by a sharp increase in contamination particle numbers. We postulate that the YO_xF_y formed on the coating surface continuously interacted with the NF_3/O_2 plasma. This caused the YO_xF_y to transform into particles and detach from the surface, exposing the AlO_x site beneath the partially covered surface of YO_xF_y. This exposed area reacted swiftly with F at the AlO_x site as in the first cycle, rapidly generating contamination particles. The significant variance in particle generation number at the plasma-off stage between cycles provided evidence for this. When Al_2O_3 and Y_2O_3 are exposed to fluorine-based plasma, F and O are substituted to form MO_xF_y (M = Al, Y), and volume expansion occurs [25]. The formation of many M − F bonds on the surface, which have lower binding energy than M − O bonds, leads to MF_x growth at weak bonding sites, such as defects within the coating, resulting in particle generation [26]. Al-F bonds possess lower binding energy than Y-F bonds [27,28]. Therefore, they primarily generate small-sized particles. The smaller the particle size, the more

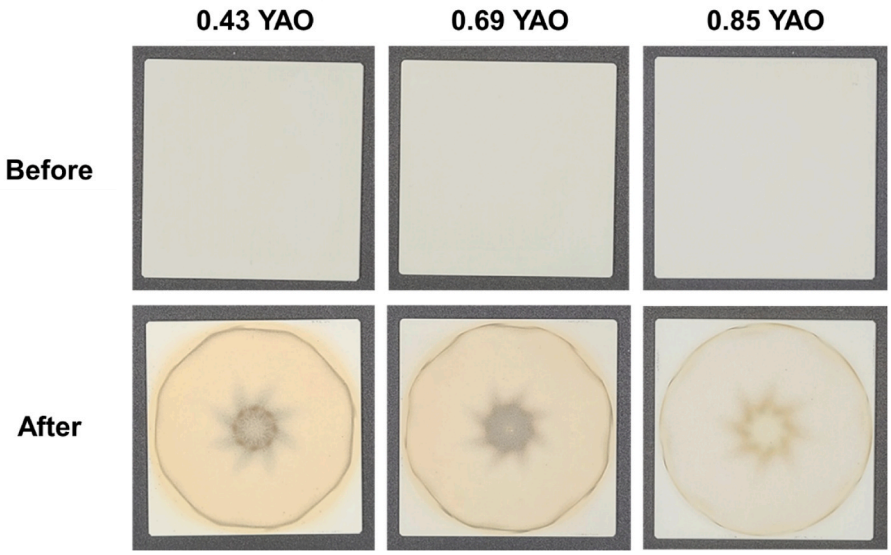

Fig. 5. Surface image of the YAO coating before and after plasma exposure.

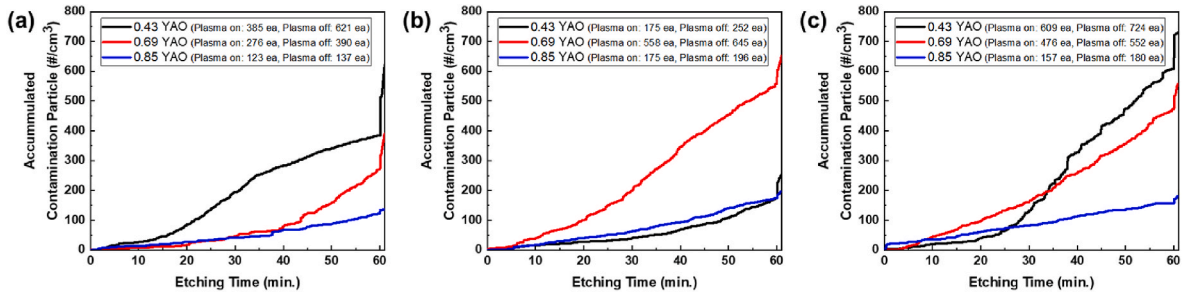

Fig. 6. Real-time detection of the concentration of accumulated contamination particles generated from YAO coatings: (a) cycle 1, (b) cycle 2, and (c) cycle 3.

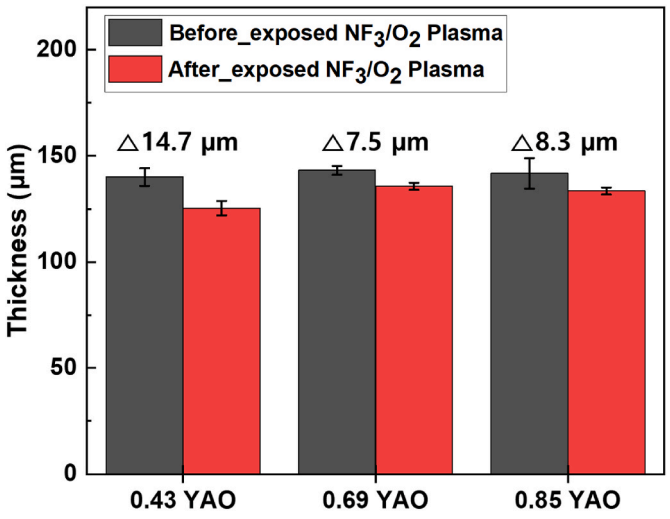

Fig. 7. Thickness of the YAO coating before and after plasma exposure.

readily they float in the plasma [29]. The floating particles are counted at the time of plasma removal. This indicates that small AlF_x particles were generated during the initial cycle and easily suspended in the plasma, and a significant number were counted upon plasma discontinuation. Conversely, the second cycle primarily produced large YF_x particles, resulting in very few particles being counted during plasma cessation. Finally, a mixture of AlF_x and YF_x was generated in the third cycle, leading to fewer particles being counted than in the first cycle but more than in the second cycle upon plasma removal.

The 0.85 YAO coating exhibited a three-fold improvement in particle generation over 0.69 YAO but suffered greater thickness loss. This is attributed to the dominant YF_x formation due to the high yttrium content ratio, resulting in larger particles, fewer particles, and a faster thickness loss rate caused by internal defect effects, such as porosity, creak, and unmelted powder within the coating. The large-sized particle generation of 0.85 YAO was evidenced by the number of particles counted at the time of plasma removal.

3.3. Investigation of plasma-resistance characteristics in 0.43 YAO with APS-Y_2O_3 bonding layer

As mentioned previously, the instability of the APS-Y_2O_3 layer used as the bonding layer contributed to the poor plasma resistance characteristics of 0.43 YAO. The metal-ceramic interface forms heterophase boundaries across ceramics and metals, primarily covalently bonded, owing to the rapid diffusion of metals. Diffusion at this interface is critical in determining the interfacial adhesion [30,31].

Typically, ceramics do not crystallize at temperatures below the glass transition temperature (T_g) without external stimuli. However, YAG crystallizes at temperatures below T_g within a few hours [25]. The rapid crystallization of YAG hampers aluminum diffusion into the ceramic, preventing the formation of a robust bond and resulting in the detachment of the YAG coating from the part. Therefore, an APS-Y_2O_3 bonding layer should be employed to maintain the aluminum content ratio and minimize the influence of the bonding layer to achieve a high-quality YAG coating. To minimize the influence of the bonding layer, we measured adhesion as a function of the APS-Y_2O_3 bonding layer thickness. Adhesion exceeded 3 MPa when the bonding layer was 30 μm or more, and the most optimal ratio was achieved when the thickness ratio of the coating (bonding layer and 0.43 YAO) was 1:4 (Table 2). To simulate an actual semiconductor manufacturing environment, samples with thickness ratios of 1:1 and 1:4 for the bonding layer (APS-Y_2O_3) and 0.43 YAO, respectively, were exposed to NF_3/O_2 gas plasma for 1 h. Subsequently, the samples were cleaned using a mixed acid solution to ascertain the reliability of the coating. This process was repeated thrice, but in the third iteration, no cleaning was performed post plasma exposure (Fig. 9). In typical semiconductor manufacturing settings, periodic cleaning of the coating surface is performed to minimize defects that may arise from the accumulation of process byproducts. The greatest difference in the number of contamination particles between the two coatings was observed after two cleaning cycles during exposure to the NF_3/O_2 gas plasma environment (Fig. 9c). As observed in Fig. 4a and 9a, the top of the coating was formed incompletely owing to the lack of hammering effect. Both samples had a total thickness of 140 μm, composed of the bonding layer and 0.43 YAO. However, there was a variation in the thickness of the bonding layer, which was 70 μm for the 1:1 ratio and 30 μm for the 1:4 ratio. Consequently, the difference in the quantity of contamination particles can be attributed to the varying film quality of the incomplete coating on the top surface. Both samples, which underwent the first round of acid-based cleaning, exhibit similar contamination particle generation. The above result could be attributed to the removal of incomplete initial surface through etching and cleaning, leading to uniform film quality. However, the samples subjected to the second acid-based cleaning showed a dramatic difference in the number of contamination particles. This discrepancy likely arose from the decrease in the thickness of 0.43 YAO owing to the two etching and cleaning processes. These procedures exposed the area affected by defects at the interface between the bonding layer and 0.43 YAO, particularly noticeable in the 1:1 sample.

YAG coatings generated smaller particles as the aluminum content ratio increased, owing to the Al_2O_3-rich site-selective reaction [18]. The number of generated particles increased, but the weight loss rate was not proportional to the aluminum content due to the defect sites within the coating. The impact of the adhesion layer should be considered when employing YAG with a high aluminum content ratio.

4. Conclusions

We subjected YAG coatings with varying aluminum and yttrium content ratios to NF_3/O_2 mixed plasma. Our findings showed that the etch rate and contamination particle characteristics, contingent on the yttrium content ratio, are governed by the selective reaction of Al_2O_3-

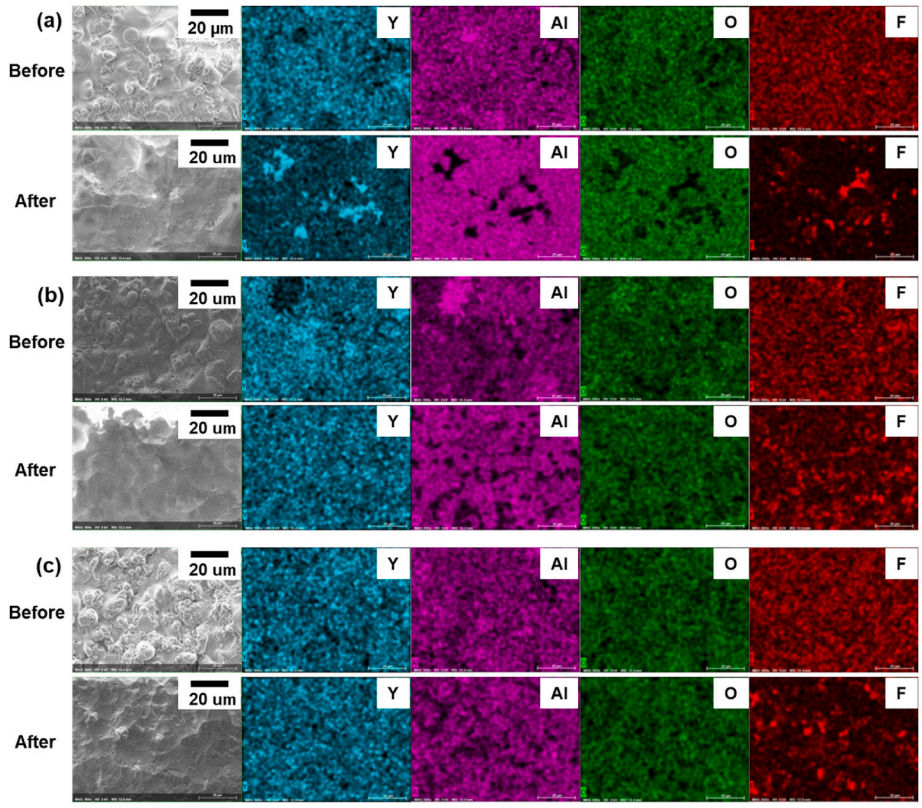

Fig. 8. EDS mapping images of the surfaces of YAO coatings: (a) 0.43 YAO, (b) 0.69 YAO, and (c) 0.85 YAO.

Table 2
Adhesion of 0.43 YAO according to layer thickness.

Layer Thickness		Adhesion [MPa]
Y_2O_3 [μm]	YAG [μm]	
10	140	0.12
20	130	1.88
30	120	3.05
40	110	2.95
50	100	3.44

rich sites and defects within the coating. With a higher aluminum content ratio (0.43 YAO), the coating exhibited fewer defects, and the initial Al_2O_3-rich sites underwent selective etching. This resulted in the dominant formation of relatively weak Al-F bonds and smaller particles. YAO with an optimal aluminum content ratio (0.69 YAO) exhibited control over the Al_2O_3-rich sites and defects in the coating. This resulted in more particles but a lower etch rate than 0.85 YAO. Conversely, when the aluminum content ratio was low (0.85 YAO), many relatively stable Y-F bonds were formed, attributed to the increased number of Y_2O_3-rich sites. This resulted in fewer particles but introduced more defects in the coating and a higher etch rate than 0.69 YAO. Moreover, actual YAG coatings dominated by the YAG phase demonstrated varied characteristics depending on the thickness ratio of the adhesion layer used to enhance the adhesion of the coating to the part.

CRediT authorship contribution statement

Jongho So: Writing – review & editing, Visualization, Conceptualization. **Eunmi Choi:** Writing – original draft, Methodology, Conceptualization. **Minjoong Kim:** Validation, Investigation, Data curation. **Dongjin Lee:** Validation, Investigation. **Jungpil Seo:** Software, Data curation. **Seonjeong Maeng:** Investigation, Data curation. **Chin-Wook Chung:** Formal analysis. **Ju-Young Yun:** Project administration, Formal analysis. **Song-Moon Suh:** Supervision, Project administration.

Declaration of competing interest

The authors declare that they have no known competing financial interests or personal relationships that could have appeared to influence

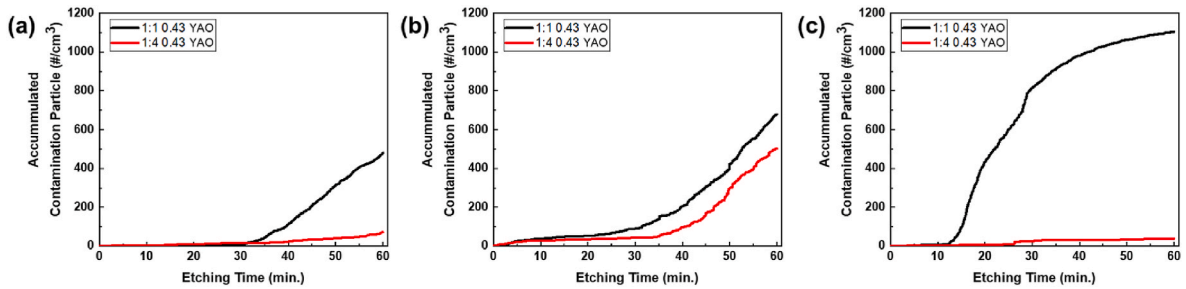

Fig. 9. Real-time detection of the concentration of accumulated contamination particles generated from 0.43 YAO coatings: (a) non-cleaning, (b) first acid-based cleaning, and (c) second acid-based cleaning.

the work reported in this paper.

Data availability

Data will be made available on request.

Acknowledgements

This research study was supported by the Characterization platform for advanced materials funded by the Korea Research Institute of Standards and Science (KRISS-2023-GP2023-0014-05).

References

[1] D.E. Ibbotson, J.A. Mucha, D.L. Flamm, J.M. Cook, Plasmaless dry etching of silicon with fluorine-containing compounds, J. Appl. Phys. 56 (1984) 2939–2942, https://doi.org/10.1063/1.333834.
[2] C. Cardinaud, Fluorine-based plasmas: main features and application in micro-and nanotechnology and in surface treatment, Compt. Rendus Chem. 21 (2018) 723–739, https://doi.org/10.1016/j.crci.2018.01.009.
[3] T.K. Lin, D.S. Wuu, S.Y. Huang, W.K. Wang, Preparation and characterization of sprayed-yttrium oxyfluoride corrosion protective coating for plasma process chambers, Coatings 8 (2018) 1–8, https://doi.org/10.3390/COATINGS8100373.
[4] J. So, E. Choi, J.T. Kim, J.S. Shin, J.B. Song, M. Kim, C.W. Chung, J.Y. Yun, Improvement of plasma resistance of anodic aluminum-oxide film in sulfuric acid containing cerium(IV) ion, Coatings 10 (2020), https://doi.org/10.3390/coatings10020103.
[5] H. Ashizawa, K. Yoshida, Plasma-resistance evaluation of yttrium oxyfluoride coating prepared by aerosol deposition method, Int. J. Appl. Ceram. Technol. 19 (2022) 375–382, https://doi.org/10.1111/ijac.13880.
[6] H. Fukumoto, I. Fujikake, Y. Takao, K. Eriguchi, K. Ono, Plasma chemical behaviour of reactants and reaction products during inductively coupled CF4 plasma etching of SiO2, Plasma Sources Sci. Technol. 18 (2009), https://doi.org/10.1088/0963-0252/18/4/045027.
[7] W.K. Wang, S.Y. Wang, K.F. Liu, P.C. Tsai, Y.H. Zhang, S.Y. Huang, Plasma etching behavior of SF6 plasma Pre-treatment sputter-deposited yttrium oxide films, Coatings 10 (2020) 1–9, https://doi.org/10.3390/coatings10070637.
[8] D.S. Lee, S. Yun, J.W. Han, M.Y. Song, Y.G. Kim, J.K. Lee, J. Choi, S. Chang, S. Hong, J.H. Kim, Microstructural evolution and mechanical properties of atmospheric plasma sprayed Y2O3 coating with state of in-flight particle, Ceram. Int. 47 (2021) 3853–3866, https://doi.org/10.1016/j.ceramint.2020.09.246.
[9] W. Tillmann, O. Khalil, M. Abdulgader, Porosity Characterization and its E Ff Ect on Thermal, Mdpi, 2019, p. 11.
[10] H. Ashizawa, K. Yoshida, Effect of the microstructures of yttria ceramics on their plasma corrosion behavior, Ceram. Int. 45 (2019) 21162–21167, https://doi.org/10.1016/j.ceramint.2019.07.093.
[11] Q. Li, J. Hu, J. Xie, X. Wang, C. Yu, S. Jiang, X. Jiang, E. Li, L. Deng, Influence of high-enthalpy atmospheric plasma spraying process parameters on microwave dielectric properties of Y2O3 coatings, J. Therm. Spray Technol. 30 (2021) 898–906, https://doi.org/10.1007/s11666-020-01144-0.
[12] S. Lee, J. Lee, W. Kim, N.M. Hwang, Plasma etching behavior of yof coating deposited by suspension plasma spraying in inductively coupled chf3/ar plasma, Coatings 10 (2020) 1–11, https://doi.org/10.3390/coatings10111023.
[13] X. Qin, G. Zhou, H. Yang, J.I. Wong, J. Zhang, D. Luo, S. Wang, J. Ma, D. Tang, Fabrication and plasma resistance properties of transparent YAG ceramics, Ceram. Int. 38 (2012) 2529–2535, https://doi.org/10.1016/j.ceramint.2011.11.023.
[14] D. Zhao, T.W. Coyle, K. Chien, Phase composition and microstructure of yttrium aluminum garnet (YAG) coatings prepared by suspension plasma spraying of Y2O3-Al2O3 powders, Surf. Coating. Technol. 235 (2013) 303–309, https://doi.org/10.1016/j.surfcoat.2013.07.058.
[15] M. Fujita, K. Morita, Plasma-resistant Member for Semiconductor Manufacturing Apparatus and Method for Manufacturing the Same, 2005.
[16] S.H. Park, K.E. Kim, S.J. Hong, Surface analysis of chamber coating materials exposed to CF4/O2 plasma, Coatings 11 (2021) 1–11, https://doi.org/10.3390/coatings11010105.
[17] B. Huang, J. Wang, Z. hua Tang, W. dong Li, W. jian Zhu, R.B. Gu, Fluoride-mediated corrosion mechanism of atmospheric-plasma-sprayed yttrium–aluminium garnet ceramic coatings, J. Eur. Ceram. Soc. 42 (2022) 6146–6158, https://doi.org/10.1016/j.jeurceramsoc.2022.06.012.
[18] Y. Tan, P. Chen, Z. Zhu, S. Wu, Z. Tian, Plasma etching behavior of yttrium-aluminum oxide composite ceramics, Int. J. Appl. Ceram. Technol. 18 (2021) 1710–1715, https://doi.org/10.1111/ijac.13712.
[19] J.B. Song, J.T. Kim, S.G. Oh, J.Y. Yun, Contamination particles and plasma etching behavior of atmospheric plasma sprayed Y2O3 and YF3 coatings under NF3 plasma, Coatings 9 (2019) 4–11, https://doi.org/10.3390/COATINGS9020102.
[20] J. So, M. Kim, H. Kwon, S. Maeng, E. Choi, C.W. Chung, J.Y. Yun, Investigation of contamination particles generation and surface chemical reactions on Al2O3, Y2O3, and YF3 coatings in F-based plasma, Appl. Surf. Sci. 629 (2023), 157367, https://doi.org/10.1016/j.apsusc.2023.157367.
[21] L. Li, F. Xie, X. Wu, J. He, S. Li, Microstructure and phase formation of atmospheric plasma sprayed YAG coatings, Surf. Coating. Technol. 466 (2023), 129614.
[22] K. Fujioka, T. Saiki, S. Motokoshi, Y. Fujimoto, H. Fujita, M. Nakatsuka, Pre-evaluation method for the spectroscopic properties of YAG bulk materials by sol–gel synthetic YAG powder, Ceram. Int. 35 (2009) 2393–2399.
[23] J. Choi, D.W. Shin, W.T. Bae, Characteristics of thermal oxidation on hot-pressed pure yttria ceramics, J. Korean Ceram. Soc. 50 (2013) 180–185, https://doi.org/10.4191/kcers.2013.50.3.180.
[24] J.B. Song, E. Choi, S.G. Oh, J.T. Kim, J.Y. Yun, Contamination particle behavior of aerosol deposited Y 2 O 3 and YF 3 coatings under NF 3 plasma, Coatings 9 (2019), https://doi.org/10.3390/coatings9050310.
[25] M. Kim, E. Choi, D. Lee, J. Seo, T.-S. Back, J. So, J.-Y. Yun, S.-M. Suh, The effect of powder particle size on the corrosion behavior of atmospheric plasma spray-Y2O3 coating: unraveling the corrosion mechanism by fluorine-based plasma, Appl. Surf. Sci. 606 (2022), 154958, https://doi.org/10.1016/j.apsusc.2022.154958.
[26] K. Miwa, N. Takada, K. Sasaki, Fluorination mechanisms of Al2O3 and Y2O3 surfaces irradiated by high-density CF4/O2 and SF6/O2 plasmas, J. Vac. Sci. Technol. A Vacuum, Surfaces, Film. 27 (2009) 831–835, https://doi.org/10.1116/1.3112624.
[27] A.J. Lichtenberg, Principles of Plasma Discharges and Materials Processing, Wiley-Interscience, 2005.
[28] M.R. Sievers, Y. Chen, P.B. Armentrout, Metal oxide and carbide thermochemistry of Y+, Zr+, Nb+, and Mo+, J. Chem. Phys. 105 (1996) 6322–6333.
[29] C. Killer, M. Mulsow, A. Melzer, Spatio-temporal evolution of the dust particle size distribution in dusty argon rf plasmas, Plasma Sources Sci. Technol. 24 (2015), https://doi.org/10.1088/0963-0252/24/2/025029.
[30] K. Burger, W. Mader, M. Rühle, Structure, chemistry and diffusion bonding of metal/ceramic interfaces, Ultramicroscopy 22 (1987) 1–13, https://doi.org/10.1016/0304-3991(87)90045-3.
[31] C.J. Li, X.T. Luo, X.Y. Dong, L. Zhang, C.X. Li, Recent research advances in plasma spraying of bulk-like dense metal coatings with metallurgically bonded lamellae, J. Therm. Spray Technol. 31 (2022) 5–27, https://doi.org/10.1007/s11666-022-01327-x.